Eur. Phys. J. B **17**, 245–251 (2000)

THE EUROPEAN PHYSICAL JOURNAL B

EDP Sciences

The microstructure of hydrogen- and deuterium-doped nanocrystalline palladium studied by small-angle neutron scattering

T. Striffler[1,a], U. Stuhr[2], H. Wipf[1], H. Hahn[3], and S. Egelhaaf[4]

[1] Institut für Festkörperphysik, Technische Universität Darmstadt, Hochschulstraße 6, 64289 Darmstadt, Germany
[2] Paul Scherrer Institut, 5232 Villigen PSI, Switzerland,
[3] Materialwissenschaft, Technische Universität Darmstadt, Petersenstraße 23, 64287 Darmstadt, Germany
[4] Institut Laue Langevin, 6 rue Jules Horowitz, BP 156, 38042 Grenoble Cedex 9, France

Received 1 May 2000

Abstract. By means of small-angle neutron scattering the microstructure of two nanocrystalline Pd samples (prepared by inert gas condensation) has been studied at room temperature in a Q-range from 10^{-3} Å^{-1} to 0.4 Å^{-1}. An additional subsequent doping of the two samples with H as well as with D (concentrations < 4 at%) caused contrast variations that provided more detailed structural information. The measured scattering intensity was modeled by a Porod contribution from large heterogenities (*e.g.* pores) and a contribution from spherical grains with a log-normal distribution of their radii. To account for the presence of grain boundaries, the grains were considered to be surrounded by a shell with a reduced Pd density and a thickness half as large as the thickness of the grain boundaries. For the above model, the data of the H-doped, D-doped and undoped sample were simultaneously fitted with one single set of adjustable parameters. The fits yielded for the two samples volume-weighted mean grain radii of 10 nm and 13 nm. The values for the grain boundary thickness lie between 0.2 and 0.8 nm. Almost all of the H- and D-atoms are, at low hydrogen concentrations, located in the grain boundaries.

PACS. 61.46.+w Clusters, nanoparticles, and nanocrystalline materials – 61.12.Ex Neutron scattering techniques (including small-angle scattering) – 61.72.Mm Grain and twin boundaries

1 Introduction

Nanocrystalline materials are polycrystals with grain sizes of a few nanometres (≈ 2–50 nm) [1–3]. The small grain sizes imply that a significant fraction of the atoms is located in or close to grain boundaries. This fact makes nanocrystalline materials a state of matter with novel physical properties.

The present paper describes a study on nanocrystalline Pd by means of small-angle neutron scattering (SANS). Small-angle neutron scattering represents an effective tool to investigate nanocrystalline structures because of the investigated Q-range from typically 10^{-3} Å^{-1} to 1 Å^{-1} ($\hbar Q$ is the momentum transfer in the scattering process, and $\hbar$ is Planck's constant). To increase the structural information in our present experiment, we additionally modified the contrast in the course of the SANS measurements by doping the investigated Pd samples subsequently with both interstitial H and D (concentrations < 4 at%; in this paper, H and D represent the two hydrogen isotopes ^{1}H and ^{2}H, whereas hydrogen stands for both isotopes). Such an aimed doping with H and D interstitials is a new method for contrast variation in studies on nanocrystalline materials.

The present procedure differs from the previous method applied for contrast variation in nanocrystalline materials where open porosities were filled by a contrast liquid, as performed in one study on nanocrystalline Pd [4]. However, most of the previous SANS experiments [5–7] on nanocrystalline materials were carried out without such a contrast variation.

Our experiments yielded information about the microstructure of the sample, such as mean grain radius and grain boundary thickness. The experiments showed also that the hydrogen interstitials are predominantly located in the grain boundaries as long as the hydrogen concentrations are low. This result was also found in an inelastic neutron scattering study [8] and in a second study

[a] e-mail: Thomas.Striffler@physik.tu-darmstadt.de

Table 1. Gas-volumetrically determined hydrogen concentrations c_{gv} and the hydrogen concentration c determined by fit from our SANS data. c_g and c_{gb} are the local concentrations in the grains and the grain boundaries, respectively, determined by fit. All concentrations are given in at%.

doping	concentrations (at%)	sample 1	sample 2
H-doping	c_{gv}	3.2	3.5
	c	3.2	2.9
	c_g	3×10^{-3}	2
	c_{gb}	28	38
D-doping	c_{gv}	3.5	1.4
	c	3.3	1.7
	c_g	7×10^{-4}	2×10^{-6}
	c_{gb}	29	71

in which the H solubility was measured in cathodically charged nanocrystalline Pd [9].

2 Experimental

We investigated two disc-shaped Pd samples (sample 1 and sample 2) prepared by inert gas condensation [1,2,10] (diameter ≈ 9.6 mm, thickness ≈ 0.5 mm, masses of 0.32 g and 0.37 g and densities of 8.66 $\frac{g}{cm^3}$ and 9.18$\frac{g}{cm^3}$ for sample 1 and sample 2, respectively). An X-ray analysis from the {111}-Bragg-peak line-broadening yielded estimates of 8 nm and 9 nm for the volume-weighted mean grain radii of sample 1 and 2, respectively. This analysis did not consider the potential influence of lattice strains so that the actual radii can be expected to be somewhat larger. Each of the samples was enclosed in a thin vacuum-sealed Al container with sapphire crystal windows for the neutrons. In the course of the SANS measurements the samples were doped with H or D by exposing them at room temperature to a H_2- or D_2-atmosphere. For such a doping the containers were filled with H_2- or D_2-gas by connecting them *via* a valve to a portable doping device which provided the H_2- or D_2-gas. The amount of gas absorbed by a sample was determined from the pressure decrease in container and doping device, which yielded the H- and D-concentrations of our samples. Table 1 presents these gas-volumetrically determined hydrogen concentrations c_{gv} of our samples, together with concentration values from the SANS results (see later).

The neutron scattering data were taken at room temperature at the ILL in Grenoble with instrument D22 [11] in a Q-range from 10^{-3} Å^{-1} to 0.4 Å^{-1}. This broad Q-range was achieved by using three different sample-detector distances (1.4 m, 8 m and 18 m) with appropriate collimation distances [11] (5.6 m, 14.4 m and 17.6 m, respectively). The wavelength of the neutrons was 10 Å.

To dope a sample in the course of the neutron scattering measurements, we had to take the container with the sample from its position in the SANS instrument, and to reposition it after the doping procedure. This repositioning of the container may have led to very small deviations of the new container position from its original position in the SANS instrument, which could have impaired the required comparability of the measurements. To investigate the potential influence of such positional changes on the measured intensity, two measurements were performed in every doping state, in which the container with the sample was, between the measurements, removed from and repositioned into the SANS instrument. We found that this taking the container from the instrument and putting it back into place did not cause any observable intensity variations in the two measurements. Consequently, the required comparability of different measurements, in particular with different doping states, can safely be assumed.

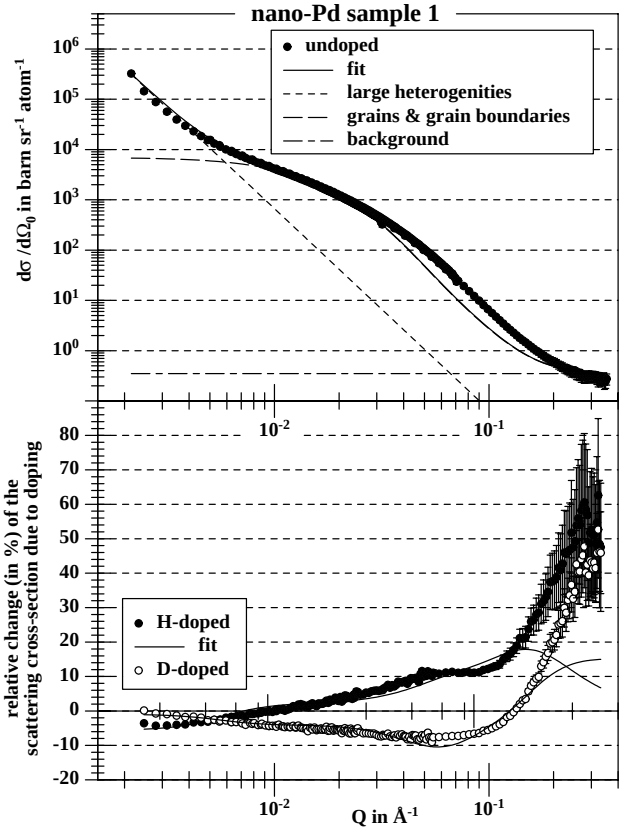

Fig. 1. Scattering cross-section $\frac{d\sigma}{d\Omega_0}$ of the undoped sample 1 (top diagram) and relative change (in %) of the scattering cross-section due to doping (bottom diagram).

3 Experimental results

The top diagrams in Figure 1 (sample 1) and Figure 2 (sample 2) present the scattering cross-sections $\frac{d\sigma}{d\Omega_0}$ per Pd atom of the undoped samples as a function of Q in a double logarithmic scale, as determined in our experiment.

The data of the doped samples are shown in the bottom diagrams of Figures 1 and 2. For the presentation of these data, we have chosen the relative change $\frac{\frac{d\sigma}{d\Omega_d} - \frac{d\sigma}{d\Omega_0}}{\frac{d\sigma}{d\Omega_0}}$

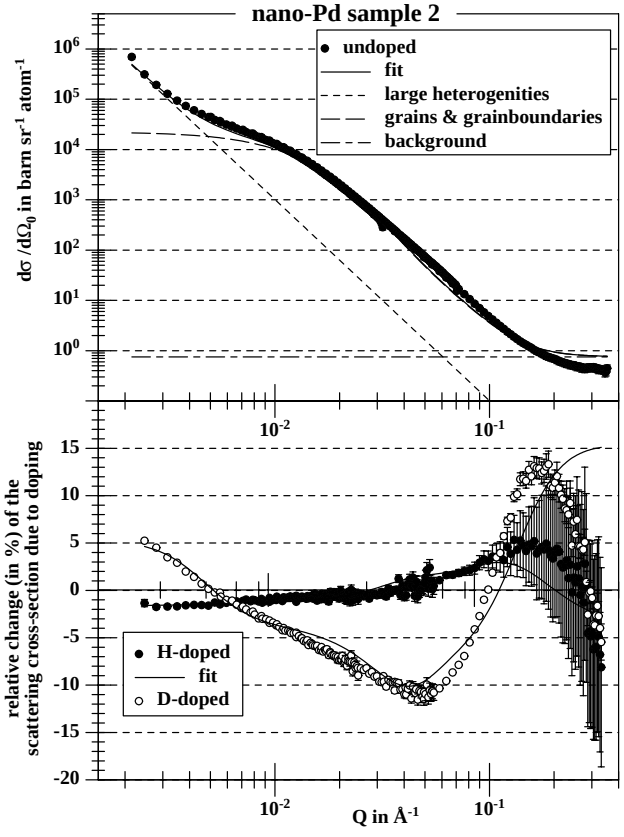

Fig. 2. Scattering cross-section $\frac{\mathrm{d}\sigma}{\mathrm{d}\Omega_0}$ of the undoped sample 2 (top diagram) and relative change (in %) of the scattering cross-section due to doping (bottom diagram).

of the scattering cross-section due to doping, where $\frac{\mathrm{d}\sigma}{\mathrm{d}\Omega_\mathrm{d}}$ is the scattering cross-section per Pd-atom of the respective doped sample. The reason for choosing this form of presentation is that the variation of the scattering cross-section due to doping is in the range of a few percent so that this variation would not be visible if we would choose the same form of data presentation as for the undoped samples.

The scattering intensity did not show any deviation from radial symmetry. Therefore, the measured intensity was radially averaged in our data analysis. Further, the measured scattering intensity was corrected (i) for background scattering from the empty sample container, under consideration of the measured transmissions, and (ii) for a Q-independent incoherent background. Finally, the scattering cross-sections per Pd-atom were determined absolutely by calibrating the measured intensity with a H_2O standard.

H- and D-doping causes a lattice expansion of $\frac{\Delta a}{a} = 0.0006$ per at% in polycrystalline Pd [12], which is accompanied by a corresponding increase of sample volume. In our experimental setup, the diameter (= 7.5 mm) of the aperture in front of the disc-shaped samples was smaller than the sample diameter. Consequently, the volume expansion of the sample due to doping decreased the number of scattering Pd-atoms in the neutron beam and thus also the scattering intensity. This effect was taken into account during the normalisation of the scattering cross-section to the number of Pd-atoms. However, the effect was very small. Even for the highest hydrogen concentration ($c_\mathrm{H} = 3.5$ at%) the decrease in the number of scattering Pd atoms was only 0.45%, using the above value for the lattice expansion also for the present nanocrystalline samples.

In order to allow a direct comparison of scattering data of a given sample in different doping states, the data of the doped sample were additionally slightly modified as described in the following:

(i) A further consequence of the lattice expansion due to hydrogen doping is that the intensity curves are shifted to smaller Q-values. Assuming a homogeneous expansion of the whole sample structure, and no other effects due to doping, we expect the scattering intensity being a function of QL, where L characterizes the sample size. In our data evaluation, this fact was considered by shifting the intensity data of the doped samples back to higher Q-values. Using the above value for H-doped lattice expansion, the maximum intensity variation due to this back shift was 2% (sample 1 at $Q = 0.0025$ Å^{-1}).

(ii) Doping the sample with H and D increases the number of incoherently scattered neutrons. These neutrons, which are scattered into the whole solid angle, reduce the high coherent SANS intensity from single scattering processes, which is of present interest and scattered in a direction close to that of the incoming beam. This reduction in the coherent SANS intensity was compensated by a multiplicative factor that increased the measured intensity. This factor is $\frac{1}{1-p}$, where p is the probability that an incoming neutron is incoherently scattered. However, the intensity changes due to this factor were so small (below 0.9%) that they had practically no importance.

4 Analysis and discussion

In the present SANS experiment, the scattering cross-section per Pd-atom is given by

$$\frac{\mathrm{d}\sigma}{\mathrm{d}\Omega} = \frac{1}{N_\mathrm{Pd}} \left| \int_{V_\mathrm{sample}} \Delta\rho \, \mathrm{e}^{\mathrm{i}\mathbf{Q}\mathbf{r}} \mathrm{d}^3\mathbf{r} \right|^2 \qquad (1)$$

where N_Pd is the number of Pd atoms and $\mathbf{r}$ is the spatial coordinate. The integration above extends over the sample volume V_sample that is exposed to the incoming neutrons. $\Delta\rho = \rho(\mathbf{r}) - \langle\rho\rangle$ is the difference between the local scattering length density $\rho(\mathbf{r})$ and mean scattering length density $\langle\rho\rangle$ of the sample. The square $\Delta\rho^2$ is called contrast.

We described our scattering data by three uncorrelated contributions to the measured intensity: (i) A first contribution from large heterogenities like pores, internal macroscopic density fluctuations and surface roughness. (ii) A second contribution caused by spherical Pd grains

with a log-normal distribution $z(R)$ of radii R, where $\int_0^\infty z(R)\,\mathrm{d}R = 1$. The log-normal distribution $z(R)$ can be described by the most probable grain radius and the width of the distribution, or alternatively by the mean grain radius and the volume-weighted mean grain radius. To model the grain boundaries, the grains were surrounded by a shell of reduced Pd density with a thickness d half as large as the grain boundary thickness. (iii) Finally a Q-independent background was considered.

The above contributions yield

$$\begin{aligned}\frac{\mathrm{d}\sigma}{\mathrm{d}\Omega} = \quad & PQ^{-4} \\ & + \frac{N_\mathrm{g}}{N_\mathrm{Pd}} \int_0^\infty z(R)\,\frac{\mathrm{d}\Sigma}{\mathrm{d}\Omega}(R)\,\mathrm{d}R \\ & + B\end{aligned} \tag{2}$$

for the scattering cross-section $\frac{\mathrm{d}\sigma}{\mathrm{d}\Omega}$ per Pd-atom where B is the Q-independent background. The first term on the right hand side of equation (2) is the contribution from the large heterogenities, approximated by Porod's law, where P is Porod's constant [14,15]. Porod's law is valid in a case in which Q is much larger than the reciprocal value of a characteristic length of the heterogenities. The second term describes the contribution of grains plus grain boundaries, where N_g and N_Pd is the number of grains and Pd-atoms, respectively. $\frac{\mathrm{d}\Sigma}{\mathrm{d}\Omega}(R)$ is the scattering cross-section of a single spherical Pd grain of radius R surrounded by a shell of reduced density and thickness d in order to account for the grain boundaries. Calculation of the scattering cross-section $\frac{\mathrm{d}\Sigma}{\mathrm{d}\Omega}(R)$ yields

$$\frac{\mathrm{d}\Sigma}{\mathrm{d}\Omega}(R) = [\Delta\rho_\mathrm{g}\, V\, f(QR) + \Delta\rho_\mathrm{gb}\, V_\mathrm{s}\, f_\mathrm{s}(QR)]^2. \tag{3}$$

In this equation, the first term in the square brackets on the right hand side represents the contribution from the grains, while the second one describes that from the grain boundaries. $V = \frac{4\pi}{3}R^3$ is the volume of a Pd grain with radius R, and $V_\mathrm{s} = \frac{4\pi}{3}\left((R+d)^3 - R^3\right)$ is that of its surrounding shell (grain boundary). $f(QR)$ and $f_\mathrm{s}(QR)$ are the form factors ([15], p. 92) of a solid sphere and a spherical shell, respectively. They can be written as

$$f(QR) = \frac{3\,[\sin(QR) - QR\cos(QR)]}{(QR)^3} \tag{4}$$

$$f_\mathrm{s}(QR) = \frac{l^3 f(Ql) - R^3 f(QR)}{l^3 - R^3}, \text{ with } l = R + d. \tag{5}$$

In equation (3) $\Delta\rho_\mathrm{g} = \rho_\mathrm{g} - \langle\rho\rangle$ and $\Delta\rho_\mathrm{gb} = \rho_\mathrm{gb} - \langle\rho\rangle$ are the scattering length density differences of the grains and the grain boundaries, respectively, where ρ_g and ρ_gb are the scattering length densities in the grains and in the grain boundaries, respectively. $\langle\rho\rangle$ is the mean scattering length density of the sample.

Our data analysis assumes that interference effects between the different scattering contributions in equation (2) are negligible. According to our knowledge, similar assumptions were in fact made in all previous studies on nanocrystalline materials (*e.g.* [4,7,13]). That interference effects can be neglected is difficult to establish theoretically, so that, in fact, the quality of our fits represents the experimental *a posteriori* justification for neglecting interference effects.

We consider first a H-doped sample. In this case the above quantities can be written as

$$\rho_\mathrm{g} = \quad n_\mathrm{Pd}\,(b_\mathrm{Pd} + c_\mathrm{g}\, b_\mathrm{H}), \tag{6}$$

$$\rho_\mathrm{gb} = \quad n_\mathrm{Pd}\, X\,(b_\mathrm{Pd} + c_\mathrm{gb}\, b_\mathrm{H}) \qquad \text{and} \tag{7}$$

$$\langle\rho\rangle = \quad \frac{N_\mathrm{g}}{V_\mathrm{sample}}\,(\langle V\rangle\,\rho_\mathrm{g} + \langle V_\mathrm{s}\rangle\,\rho_\mathrm{gb}). \tag{8}$$

In these equations, n_Pd is the particle density (particles per volume) of Pd-atoms in the grains, which is assumed to be the same as for crystalline Pd (6.79×10^{22} $\frac{\text{atoms}}{\text{cm}^3}$ in the absence of hydrogen). $b_\mathrm{Pd} = 5.91$ fm and $b_\mathrm{H} = -3.74$ fm are the coherent scattering lengths of Pd and H, respectively. The ratio of the Pd-density in the grain boundaries to the Pd-density in the grains is described by X. c_g and c_gb are the $\frac{\mathrm{H}}{\mathrm{Pd}}$-ratios in the grains and in the grain boundaries, respectively.

In the case of a D-doped sample, analogous equations apply, with the scattering length $b_\mathrm{D} = 6.67$ fm for D instead of b_H. Further, c_g and c_gb represent the $\frac{\mathrm{D}}{\mathrm{Pd}}$-ratios in the grains and in the grain boundaries, respectively. Finally c_g and c_gb are assumed to be zero for the description of the undoped samples.

The solid curves in Figures 1 and 2 are the result of *simultaneously* fitting the three data sets of each sample (data of the H-doped, D-doped and undoped sample), using identical fitting parameters.

We consider first the upper diagrams of Figures 1 and 2, which present the scattering cross-sections of the undoped samples. These diagrams show the total scattering cross-section and the three different individual scattering contributions caused by large heterogenities (*e.g.* pores), grains plus grain boundaries and background, respectively. It can be seen that the intensity at small Q-values results mainly from large heterogenities and is well described by Porod's law. On the other hand, the intensity is dominated by scattering from grains and grain boundaries in the Q-region between 10^{-2} and 10^{-1} Å^{-1}.

We discuss now the intensity behaviour of the doped samples, shown in the bottom diagrams of Figures 1 and 2. At small Q-values, the intensities of the H-doped samples are lower than those of the D-doped samples. This behaviour can be explained by the assumption that a noticeable fraction of the intensity at small Q-values is caused by pores as shown in the following. Doping the samples with H decreases the mean scattering length density $\langle\rho\rangle$, because of the negative scattering length ($b_\mathrm{H} = -3.74$ fm) of H and the positive scattering length of Pd ($b_\mathrm{Pd} = 5.91$ fm). Therefore, the presence of H lowers the contrast of the pores, which do not contain H, so that H-doping decreases the scattering intensity at small Q-values. In contrast to this, a doping with D increases the intensity at small Q-values because of its positive scattering length ($b_\mathrm{D} = 6.67$ fm).

The fact that our data are so well described by Porod's law at low Q-values does not allow making statements on the size of the pores in our samples. Even if we assume that (i) the whole intensity at low Q-values is caused by pores and that (ii) this intensity can be modeled by spherical pores having a log-normal radii distribution described by a mean pore radius $\langle R_\mathrm{p}\rangle$ and a distribution width σ, it is not possible to determine the two quantities $\langle R_\mathrm{p}\rangle$ and σ from the single experimental value of Porod's constant. In the limit of small distribution widths σ, for instance, our values for the mean mean pore radii $\langle R_\mathrm{p}\rangle$ yield $\approx$ 800 nm and $\approx$ 1 400 nm for sample 1 and sample 2, respectively (considering the densities given in the beginning of Sect. 2). If the distribution widths σ are assumed to be larger, we find smaller values for the mean pore radii $\langle R_\mathrm{p}\rangle$. For $\sigma \approx 1$ the mean pore radius $\langle R_\mathrm{p}\rangle$ is 133 nm, as reported in a previous SANS study [4].

In contrast to the intensity behaviour at small Q-values, the intensity of the H-doped samples is in the Q-region between 10^{-2} and 10^{-1} Å^{-1} higher than that of the D-doped samples. This results from the fact (i) that, in the considered Q-region, the intensity contribution from the grains is much bigger than that from the grain boundaries, and (ii) that almost all of the H and D is found to be in the grain boundaries. This follows from our fits and is discussed quantitatively later. Qualitatively, we can understand the differences for the two hydrogen isotopes as follows. Let us consider first a doping with H which lowers the mean scattering length density $\langle\rho\rangle$ because of the negative scattering length of H. The scattering length density ρ_g in the grains does not change, if, as assumed above, almost all of the H is in the grain boundaries. Accordingly H-doping increases the contrast $\Delta\rho_\mathrm{g}$ of the grains, so that the intensity increases in the considered Q-region. In contrast to this, D-doping decreases the intensity because of its positive scattering length.

We discuss now the quantitative results of our fits. The local hydrogen concentrations c_g and c_gb in the grains and the grain boundaries, respectively, are listed in Table 1, whereas the other values determined by fit are presented in Table 2. The fits yielded for sample 1 a mean grain radius of 6 nm and a volume-weighted mean grain radius of 10 nm. For sample 2 the corresponding values are 8 nm and 13 nm. The values of the volume-weighted mean grain radii show reasonable agreement with the radii determined in the X-ray analysis as discussed in the beginning of Section 2 (8 nm for sample 1 and 9 nm for sample 2; this agreement would be even better if an additional Bragg-peak line-broadening caused by lattice strains would have been taken into account in the evaluation of the X-ray data). The fits were not very sensitive to the grain boundary thickness $2d$, and the values we found for this quantity lie between 0.2 and 0.8 nm. For the ratio X, *i.e.* the ratio of Pd particle density in the grain boundaries to Pd particle density in the grains, the fits yielded $X \approx 0.77 \pm 0.08$ and $X \approx 0.68 \pm 0.07$ for sample 1 and for sample 2, respectively.

The values for Porod's constant P in Table 2 change slightly between different doping states because the contrast of the large heterogenities is expected to change on hydrogen doping. However, these changes are less than 6% for each sample and are, therefore, smaller then the experimental accuracy for our scattering data (at the lowest Q-value $\approx$ 10%).

Table 2. Results determined by our fits (the results for the hydrogen concentration are listed in Tab. 1).

	sample 1	sample 2
mean grain radius	6 nm	9 nm
volume weighted mean grain radius	10 nm	13 nm
$2d$	0.8 nm	0.2 nm
X	0.77 ± 0.08	0.68 ± 0.07
B_undoped	$0.35 \frac{\mathrm{barn}}{\mathrm{sr\ atom}}$	$0.75 \frac{\mathrm{barn}}{\mathrm{sr\ atom}}$
$B_\mathrm{H-doped}$	$0.35 \frac{\mathrm{barn}}{\mathrm{sr\ atom}}$	$0.72 \frac{\mathrm{barn}}{\mathrm{sr\ atom}}$
$B_\mathrm{D-doped}$	$0.40 \frac{\mathrm{barn}}{\mathrm{sr\ atom}}$	$0.86 \frac{\mathrm{barn}}{\mathrm{sr\ atom}}$
P_undoped	$6.66 \frac{10^{-6}\ \mathrm{barn}}{\mathrm{Å}^4\ \mathrm{sr\ atom}}$	$1.01 \frac{10^{-5}\ \mathrm{barn}}{\mathrm{Å}^4\ \mathrm{sr\ atom}}$
$P_\mathrm{H-doped}$	$6.29 \frac{10^{-6}\ \mathrm{barn}}{\mathrm{Å}^4\ \mathrm{sr\ atom}}$	$1.00 \frac{10^{-5}\ \mathrm{barn}}{\mathrm{Å}^4\ \mathrm{sr\ atom}}$
$P_\mathrm{D-doped}$	$6.60 \frac{10^{-6}\ \mathrm{barn}}{\mathrm{Å}^4\ \mathrm{sr\ atom}}$	$1.07 \frac{10^{-5}\ \mathrm{barn}}{\mathrm{Å}^4\ \mathrm{sr\ atom}}$

Although the expected incoherent scattering caused by Pd and the hydrogen that we added by doping had been subtracted from our data, the data show an intensity contribution at high Q-values that cannot be described by considering solely contributions from large heterogenities, grains and grain boundaries. We assume that this intensity contribution reflects scattering due to structural disorder in our samples and incoherent scattering from gases, like H, and water vapor adsorbed in our samples already before hydrogen doping. We accounted for this intensity contribution by assuming a Q-independent background B. The results for B are presented in Table 2. These values of B are generally somewhat smaller than those reported for a similar Q-independent background in a study [13] on nanocrystalline Si-Au alloys. Finally it should be mentioned that the intensity contribution modeled by B is of relevance only at the highest Q-values of our study.

According to Table 1, the values for the local concentrations c_gb in the grain boundaries lie between 28 at% and 71 at%. Comparing these values with the local concentrations c_g in the grains, one can see that almost 100% of the absorbed H and D is located in the grain boundaries. This is an important result from the present SANS measurement, also found in an inelastic neutron scattering study [8] and in a second study in which the H solubility was measured in cathodically charged nanocrystalline Pd [9]. The fact that almost 100% of the absorbed H and

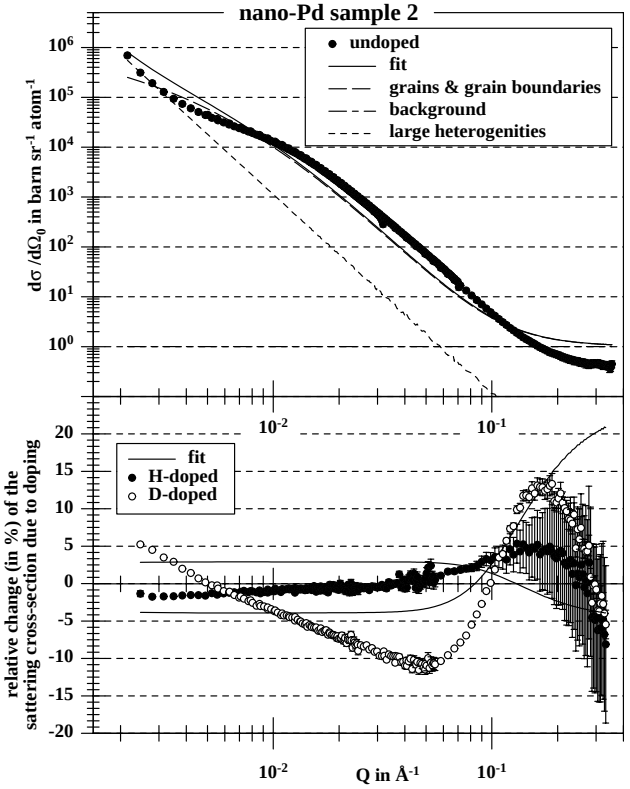

Fig. 3. Fit with the assumption that no H or D are in the grain boundaries.

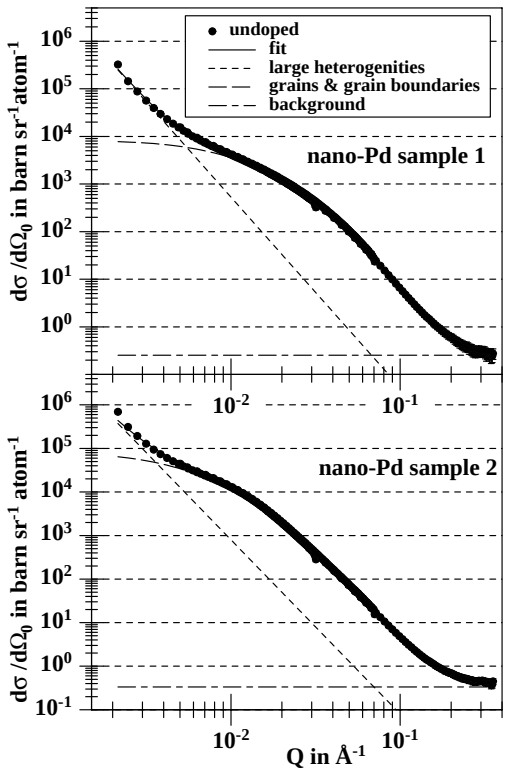

Fig. 4. Fits solely to the data of the undoped samples.

D is located in the grain boundaries, holds for all of our measurements except for the measurement of sample 2 in H-doped state which has the highest H concentration of all of our measurements. For this measurement the fit yielded a local H concentration c_{g} in the grains of 2 at%, so that not all of the H is located in the grain boundaries. A point to consider here is the accuracy of the concentration values determined from our fits, particularly those of sample 2. For this sample the concentration values determined by our fit are not very reliable, which is exemplified by the fact that the total concentrations c_{gv} determined gas-volumetrically and c determined by our fits differ by about 20%. If we consider a similar uncertainty also for the other concentrations determined by our fit for sample 2, it seems doubtful whether the difference in the grain boundary concentrations c_{gb} for the two isotopes H and D are really significant.

Figure 3 presents the result of an additional fit performed with the specific assumption that no H or D were in the grain boundaries. Especially the bottom diagrams of this figure indicate clearly that the fitted curves describe the data unsatisfactorily under this assumption. This shows that a description of the measured data is only possible if almost all of the H and D is in fact located in the grain boundaries.

As already mentioned, a single set of parameters was *simultaneously* fitted, for each sample, to the data of its H-doped, D-doped and undoped state. This makes a less perfect data description understandable, compared to previous fits [4,6] where only the data of undoped samples have been fitted. Under consideration of this fact, we consider our fits as satisfactory, and this the more because of the reasonable agreement between the volume-weighted mean grain radii and the values found by X-ray analysis. Further, the values of the total H- and D-concentrations c, agree quite well with those c_{gv} determined gas-volumetrically, as can be seen in Table 1.

Finally we point out that our fits yielded a perfect description, as previous studies [4,6] did, if we consider only the data of a given sample in a single doping state (for instance in the undoped state). This can be seen in Figure 4 which shows fits solely to the data of the two samples in an undoped state. These fits yielded a mean grain radius of 2 nm and a volume-weighted radius of 7 nm for sample 1. For sample 2 we found a mean grain radius of 4 nm and a volume-weighted radius of 14 nm. The values of the mean grain radii are smaller than those found by our simultaneous fits, whereas the widths of the radii distributions are larger. Although the fits in Figure 4 describe the data of the undoped samples very well, their results for the fitting parameters are less reliable than those found by our simultaneous fits. One reason is that the parameter values found by the fits in Figure 4 are not able to describe the data of the doped samples. Secondly, the agreement between the volume-weighted mean grain radii found by the fits in Figure 4 and those found by our X-ray analysis is extremely poor, in contrast to the agreement

the volume-weighted mean grain radii from our simultaneous fits show.

5 Conclusion

We investigated the microstructure of two nanocrystalline Pd samples using SANS. To increase structural information, an additional contrast variation was performed by aimed H- and D-doping of the samples. We modeled the measured scattering cross-sections by a Porod contribution from large heterogenities (*e.g.* pores) and a second contribution caused by grains and grain boundaries. This second contribution was modeled by spherical grains having a log-normal distribution of their radii. Thin shells of reduced Pd density enveloping the grains served as a model for the grain boundaries. Simultaneous fits to the data of a given sample in H-doped, D-doped and undoped state with only one set of parameters yielded information about the mean grain radius and the grain boundary thickness. We found that almost all of the H and D is located in the grain boundaries, confirming the result of previous studies using other experimental methods [8,9].

This work has been funded by the German Federal Ministry of Education and Research (BMBF) under the contract number 03-WI5DAR-8.

References

1. H. Gleiter, Progr. Mater. Sci. **33**, 223 (1989).
2. R. Siegel, in *Materials Science and Technology*, edited by R.W. Cahn, P. Haasen, E.J. Kramer (Weinheim, 1991), Vol. 15, p. 583.
3. H. Gleiter, Adv. Mater. **4**, 474 (1992).
4. S. Janßen, J. Wagner, H. Natter, J. Prewo, R. Rupp, J. Löffler, H. Eckerlebe, R. May, G. Meier, R. Hempelmann, Nanostruct. Mater. **9**, 327-330 (1997).
5. E. Jorra, H. Franz, J. Peisl, G. Wallner, W. Petry, R. Birringer, H. Gleiter, T. Haubold, Philos. Mag. B **60**, 159 (1989).
6. P.G. Sanders, J.R. Weertman, J.G. Barker, R.W. Siegel, Scrip. Metall. Mat. **29**, 91 (1993).
7. W. Wagner, *et al.*, J. Mater. Res **6**, 2193 (1991).
8. U. Stuhr, H. Wipf, T.J. Udovic, J. Weißmüller, H. Gleiter, J. Phys. Cond. Matter **7**, 219 (1995).
9. Mütschele, R. Kirchheim, Scripta Metall. **21**, 135 (1987).
10. C.G. Granqvist, R.A. Buhrmann, J. Appl. Phys. **47**, 2200 (1976).
11. `http://www.ill.fr/YellowBook/D22`.
12. H. Peisl, in *Hydrogen in Metals I*, edited by G. Alefeld, J. Völkl (Springer Verlag, 1978), Vol. 28, p. 69.
13. A. Wiedenmann, A. Sturm, H. Wollenberger, Mat. Sci. Eng. **A179/A180**, 458-463 (1994).
14. G. Porod, Kolloid-Z. **124**, 83-114 (1951).
15. G. Porod, in *Small-Angle X-ray Scattering* edited by O. Glatter, O. Kratky (Academic Press, London, 1982).